Turing pattern formation in fractional activator-inhibitor systems

B. I. Henry* and T. A. M. Langlands
Department of Applied Mathematics, School of Mathematics, University of New South Wales, Sydney NSW 2052, Australia

S. L. Wearne†
Department of Biomathematical Sciences, Mount Sinai School of Medicine, New York, New York 10029-6574, USA
(Received 31 January 2005; published 1 August 2005)

Activator-inhibitor systems of reaction-diffusion equations have been used to describe pattern formation in numerous applications in biology, chemistry, and physics. The rate of diffusion in these applications is manifest in the single parameter of the diffusion constant, and stationary Turing patterns occur above a critical value of d representing the ratio of the diffusion constants of the inhibitor to the activator. Here we consider activator-inhibitor systems in which the diffusion is anomalous subdiffusion; the diffusion rates are manifest in both a diffusion constant and a diffusion exponent. A consideration of this problem in terms of continuous-time random walks with sources and sinks leads to a reaction-diffusion system with fractional order temporal derivatives operating on the spatial Laplacian. We have carried out an algebraic stability analysis of the homogeneous steady-state solution in fractional activator-inhibitor systems, with Gierer-Meinhardt reaction kinetics and with Brusselator reaction kinetics. For each class of reaction kinetics we identify a Turing instability bifurcation curve in the two-dimensional diffusion parameter space. The critical value of d, for Turing instabilities, decreases monotonically with the anomalous diffusion exponent between unity (standard diffusion) and zero (extreme subdiffusion). We have also carried out numerical simulations of the governing fractional activator-inhibitor equations and we show that the Turing instability precipitates the formation of complex spatiotemporal patterns. If the diffusion of the activator and inhibitor have the same anomalous scaling properties, then the surface profiles of these patterns for values of d slightly above the critical value varies from smooth stationary patterns to increasingly rough and nonstationary patterns as the anomalous diffusion exponent varies from unity towards zero. If the diffusion of the activator is anomalous subdiffusion but the diffusion of the inhibitor is standard diffusion, we find stable stationary Turing patterns for values of d well below the threshold values for pattern formation in standard activator-inhibitor systems.

DOI: 10.1103/PhysRevE.72.026101 PACS number(s): 82.40.Ck, 89.75.Kd, 05.40.−a, 82.39.Rt

I. INTRODUCTION

One of the best understood theoretical mechanisms for pattern formation is the Turing instability [1] of a homogeneous steady state in a two-species reaction-diffusion system. On its own, diffusion tends to smooth out irregularites; however, the differential diffusion of two distinct species coupled by nonlinear reaction terms may result in certain wavelengths becoming unstable so that patterns are produced. This model for pattern formation has recently found support in numerous applications in biology [2,3], chemistry [3,4], neuroscience [5], physics [6], and optics [7,8]. As an example, Turing pattern formation in activator-inhibitor systems provides a credible theoretical explanation of animal coat patterns [9] that can also explain the occurrence of different coat patterns on clones [10].

The general form of the two-species reaction-diffusion model is [9]

$$\frac{\partial n_1(\mathbf{x},t)}{\partial t} = \lambda f_1(n_1,n_2) + \nabla^2 n_1(\mathbf{x},t), \tag{1}$$

$$\frac{\partial n_2(\mathbf{x},t)}{\partial t} = \lambda f_2(n_1,n_2) + d\nabla^2 n_2(\mathbf{x},t). \tag{2}$$

In these equations, $n_1(\mathbf{x},t)$ and $n_2(\mathbf{x},t)$ are the number densities for the two species, f_1 and f_2 are (generally nonlinear) functions describing the reaction kinetics, d is the ratio of the diffusion coefficients of species 2 to species 1, and $\lambda > 0$ is a scaling variable which can be interpreted as the characteristic size of the spatial domain or as the relative strength of the reaction terms.

The standard reaction-diffusion model is a diffusion-limited process in which the time for reactions to occur within a given reaction zone is considered to be much less than the time for reactants to diffuse between reaction zones. The reaction-diffusion model is also a mean-field model in which it is assumed that the reactions do not themselves introduce correlations between the diffusing species but are dependent only on local average concentrations; thus microscopic fluctuations in $n(\mathbf{x},t)$ at the atomic level are ignored [11]. If the concentration of species is spatially homogeneous, then the reaction-diffusion model reduces to the classical macroscopic rate equations from the law of mass action (see, e.g., [12]).

The canonical model for Turing instability induced pattern formation is a reaction-diffusion equation with activator-inhibitor reaction kinetics—i.e., Eqs. (1) and (2) with

*Electronic address: B.Henry@unsw.edu.au
†Also at Fishberg Research Center for Neurobiology, Computational Neurobiology and Imaging Center. Electronic address: susan@camelot.mssm.edu

$\partial f_2/\partial n_1 > 0$ and $\partial f_1/\partial n_2 < 0$. In this case species 1 is an activator for production of species 2, and species 2 is an inhibitor for production of species 1. A simple linear stability analysis about the homogeneous steady-state solution, $n_1^\star, n_2^\star$, reveals that necessary conditions for Turing instability induced pattern formation are [9]

$$a_{11} + a_{22} < 0, \tag{3}$$

$$a_{11}a_{22} - a_{12}a_{21} > 0, \tag{4}$$

$$d > \left(\frac{1}{a_{11}} [\sqrt{a_{11}a_{22} - a_{12}a_{21}} + \sqrt{-a_{12}a_{21}}] \right)^2, \tag{5}$$

where $a_{ij} = \partial f_i/\partial n_j$ is evaluated at the homogeneous steady-state solution. If the above conditions are met, then it can be shown that there is a range of wave numbers q defined by [9]

$$\frac{1}{2d}[(da_{11} + a_{22}) - \sqrt{(da_{11} + a_{22})^2 - 4d(a_{11}a_{22} - a_{12}a_{21})}] \leqslant q^2 \leqslant \frac{1}{2d}[(da_{11} + a_{22}) + \sqrt{(da_{11} + a_{22})^2 - 4d(a_{11}a_{22} - a_{12}a_{21})}], \tag{6}$$

which will become excited and thus produce patterns. A necessary requirement for pattern formation consistent with the conditions, Eqs. (3)–(5), is that the inhibitor diffuse faster than the activator ($d > 1$) in all activator-inhibitor systems. Indeed in many modeling applications the required diffusion ratio from Eq. (5) is more than an order of magnitude whereas most chemical species in aqueous solutions have diffusion ratios within a factor of 2. The first experimental evidence for Turing pattern formation in an activator-inhibitor system [4] was subsequently revealed to be influenced by spatial inhomogeneities (arising from the colour indicator in the reactor gel) that effectively lowered the diffusion constant of the activator [13] so that very large diffusion ratios were realized. However, the general theoretical requirement of large diffusion ratios is still an impediment for accepting the Turing pattern formation paradigm in many applications.

In recent years numerous physical and biological systems have been reported in which the diffusion rates of species cannot be characterized by the single parameter of the diffusion constant. Instead, the (anomalous) diffusion is characterized by a scaling parameter α as well as a diffusion constant D, and the mean-square displacement of diffusing species $\langle r^2(t) \rangle$ scales as a nonlinear power law in time—i.e., $\langle r^2(t) \rangle \sim t^\alpha$. As examples, single-particle tracking experiments and photobleaching recovery experiments have revealed subdiffusion ($0 < \alpha < 1$) of proteins and lipids in a variety of cell membranes [14–18]. Moreover, anomalous subdiffusion (the case with $0 < \alpha < 1$) is generic in media with obstacles [19] or binding sites [20].

In this paper we investigate the effects of subdiffusion on Turing pattern formation in model activator-inhibitor systems in the diffusion-limited regime with fast reactions. To simplify the theoretical analysis we have restricted our attention to systems in which the concentrations vary in only one spatial direction. This limits the direct application of our results to a particular model system with known reaction kinetics since in one-dimensional space the diffusion is not an effective mechanism for mixing and this in turn produces anomalous kinetics [21]. However, from the point of view of direct applications we could consider a higher-dimensional spatial system in which concentration variations are primarily in one spatial direction or a one-dimensional spatial system in which the prescribed reaction kinetics incorporates the anomalous kinetics behavior.

A consideration of the problem of anomalous subdiffusion with reactions in terms of continuous-time random walks (CTRWs) with sources and sinks leads to a fractional activator-inhibitor model with a fractional order temporal derivative operating on the spatial Laplacian [22–28]. A similar type of system has also been proposed for diffusion with reactions on a fractal [29]. The problem of anomalous superdiffusion with reactions has also been considered and in this case a fractional reaction-diffusion model has been proposed with the spatial Laplacian replaced by a spatial fractional differential operator [30].

If the reaction time is not short compared with the diffusion time in subdiffusive systems with reactions (for example, if many encounters between reactants are required before reactions proceed), then an alternate model has been proposed where the fractional order temporal derivative operates on both the spatial Laplacian and the reaction term [31–33]. An important distinction between the two anomalous reaction-diffusion models becomes apparent when the concentration of species is spatially homogeneous; this latter model does not reduce to the classical macroscopic rate equations except when the diffusion is also nonanomalous.

The dynamics of reaction fronts between initially separated species in reaction-diffusion systems with anomalous diffusion has been studied extensively [25,26,31–33]. In this paper we investigate Turing pattern formation in reaction-diffusion models with anomalous subdiffusion incorporated through the fractional order temporal derivative operating on the Laplacian. In the initial state for this problem the species are distributed almost homogeneously in space. We have investigated the effects of both Gierer-Meinhardt reaction kinetics [34] and Brusselator reaction kinetics [35]. Some preliminary results from this study were reported recently in a conference report [27]. In recent work, Varea and Barrio [36] have examined Turing pattern formation in reaction-diffusion models with anomalous diffusion incorporated through fractional order spatial derivatives operating on the Laplacian. An important finding of their work is that nonstationary Turing patterns occur with the velocity of the moving patterns dependent on the exponent of the fractional differential operator.

The summary findings from the present study are as follows: (i) Turing instabilities occur in fractional activator-inhibitor systems for all values of the anomalous diffusion scaling exponent α. The critical value of the ratio of diffusion coefficients (inhibitor to activator) for Turing instabilities decreases monotonically as the diffusion becomes more subdiffusive. (ii) Turing instabilities precipitate spatiotemporal patterning in fractional activator-inhibitor systems. The surface profiles for the patterns vary from smooth to rough as

the diffusion scaling exponent α decreases from unity (standard diffusion) towards zero (extreme subdiffusion). (iii) If there is standard diffusion for the inhibitor but anomalous subdiffusion for the activator, then stationary Turing patterns can occur for diffusion constant ratios (inhibitor to activator) much less than those required by linear stability analysis with standard diffusion in both the activator and the inhibitor. This important result has also recently been reported in a related study by Weiss [37] using Monte Carlo simulations of subdiffusive random walks with reactions.

The remainder of this paper is organized as follows: In Sec. II we introduce the fractional activator-inhibitor system from the continuous-time random walk formalism with sources and sinks. In Sec. III we carry out linear stability analysis of the homogeneous steady-state solutions and we obtain algebraic results for the critical value of the ratio of diffusion coefficients (inhibitor to activator) for Turing instabilities over a range of α in fractional activator-inhibitor systems. Turing instability bifurcation curves are derived from this analysis for both Gierer-Meinhardt reaction kinetics and Brusselator reaction kinetics. We also identify the dominant excited modes from the linear stability analysis. In Sec. IV we describe the results of our numerical simulations of pattern formation in fractional activator-inhibitor equations. We conclude with a discussion and summary in Sec. V.

II. FRACTIONAL ACTIVATOR-INHIBITOR MODEL

The asymptotic properties that characterize anomalous subdiffusion can be modeled at the mesoscopic level using continuous-time random walks [38] with the spatial and temporal probability density functions decoupled and with temporal memory represented through a power-law waiting time distribution [39]

$$\psi(t) \sim t^{-1-\gamma}. \tag{7}$$

The power-law waiting time distribution is an example of a so-called long-tailed distribution characterizing sporadic behavior with short bursts of events occurring frequently but also with very long pauses between events occurring occasionally. The CTRW model with a power-law waiting time distribution can be reformulated as a fractional diffusion equation [40–43]. In a similar fashion, anomalous subdiffusion in an external field has been modeled using a fractional Fokker-Planck equation [43,44] and anomalous subdiffusion with sinks and sources has been modeled using fractional reaction-diffusion equations [22–25,27,28]. The evolution equation for the number density of walkers, $n(\mathbf{x},t)$, in the CTRW formulation of this problem is [22,25]

$$n(\mathbf{x},t) = \Phi(t)n(\mathbf{x},0) + \sum_{\mathbf{x}'}\int_0^t \Psi(\mathbf{x}-\mathbf{x}',t-t')n(\mathbf{x}',t')dt' + \int_0^t \Phi(t-t')g(\mathbf{x},t')dt', \tag{8}$$

where $\Phi(t)$ is the survival probability that walkers remain at their starting locations after time t; the second term on the right-hand side represents the number density of walkers that arrive at $\mathbf{x}$ at time t after a random walk from locations $\mathbf{x}'$ at times t'. The function $\Psi(\mathbf{x},t)$ denotes the transition probablity distribution for a step of length $\mathbf{x}$ in the time interval $t,t+dt$. The final term on the right-hand side is the source (sink) term to account for increases (decreases) in the number density at $\mathbf{x}$ and t due to reactions. The evolution equation simplifies under the assumption that the waiting time between random walks and the step lengths of the random walks are independent. In this case we can write $\Psi(\mathbf{x}-\mathbf{x}',t-t')=\sigma(\mathbf{x}-\mathbf{x}')\psi(t-t')$ and $\Phi(t)=1-\int_0^t\psi(t')dt'$. If it is also assumed that the waiting time distribution $\psi(t)$ is governed by a power law as in Eq. (7) (for anomalous subdiffusion) but the step length distribution $\sigma(\mathbf{x})$ has finite moments, then the evolution equation that describes the long-time behavior can be written as [22]

$$u\hat{n}(\mathbf{x},u) - n(\mathbf{x},0) = Cu^{1-\gamma}\nabla^2\hat{n}(\mathbf{x},u) + \hat{n}(\mathbf{x},u), \tag{9}$$

where $\hat{n}$ denotes the temporal Laplace transform of n and $u<1$ is the transform variable. A fractional reaction-diffusion equation then results after inverting the Laplace transform and noting that (see, e.g., Sec. 2.8 of [45])

$$u^\alpha\hat{y}(u) = \mathcal{L}({}_0D_t^\alpha y(t)) + [{}_0D_t^{\alpha-1}y(t)]|_{t=0}, \tag{10}$$

where

$${}_0D_t^\alpha y(t) = \frac{d}{dt}\left(\frac{1}{\Gamma(1-\alpha)}\int_0^t \frac{y(s)}{(t-s)^\alpha}ds\right) \tag{11}$$

is the Riemann-Liouville fractional derivative with $0<\alpha<1$ and $\mathcal{L}$ denotes the temporal Laplace transform. Alternate formulations in terms of the Grünwald-Letnikov fractional derivative

$${}^{GL}D_t^\alpha y(t) = \lim_{h\to 0}\frac{1}{h^\alpha}\sum_{j=0}^{\infty}(-1)^j\frac{\Gamma(\alpha+1)}{\Gamma(j+1)\Gamma(\alpha-j+1)}y(t-jh) \tag{12}$$

or the Caputo fractional derivative

$${}_0^CD_t^\alpha y(t) = \frac{1}{\Gamma(1-\alpha)}\int_0^t \frac{\frac{d}{ds}y(s)}{(t-s)^\alpha}ds \tag{13}$$

are also possible using the relations (see, e.g., Sec. 2.8 of [45])

$$u^\alpha\hat{y}(u) = \mathcal{L}({}^{GL}D_t^\alpha y(t)) \tag{14}$$

and

$$u^\alpha\hat{y}(u) = \mathcal{L}({}_0^CD_t^\alpha y(t)) + u^{\alpha-1}y(0), \tag{15}$$

respectively.

A special case of the fractional reaction-diffusion equation is the fractional activator-inhibitor system [23]

$$\frac{\partial n_1(x,t)}{\partial t} = \lambda f_1(n_1,n_2) + \mathcal{D}^{1-\gamma_1}n_1(x,t), \tag{16}$$

$$\frac{\partial n_2(x,t)}{\partial t} = \lambda f_2(n_1,n_2) + d\mathcal{D}^{1-\gamma_2} n_2(x,t), \tag{17}$$

where $n_1(x,t)$ and $n_2(x,t)$ denote the concentrations of the activator and inhibitor, respectively; $0<\gamma_1\leqslant 1$ is the anomalous diffusion exponent of the activator, and $0<\gamma_2\leqslant 1$ is the anomalous diffusion exponent of the inhibitor. The reaction kinetics is defined by the functions $f_1(n_1,n_2)$ and $f_2(n_1,n_2)$. The fractional differential operator is given by

$$\mathcal{D}^{1-\gamma} n(x,t) = \frac{\partial^{1-\gamma}}{\partial t^{1-\gamma}} \nabla^2 n(x,t) + \mathcal{L}^{-1}\left(\frac{\partial^{-\gamma}}{\partial t^{-\gamma}} \nabla^2 n(x,t)\big|_{t=0} \right), \tag{18}$$

where

$$\frac{\partial^{-\gamma} y(t)}{\partial t^{-\gamma}} = \left(\frac{1}{\Gamma(\gamma)} \int_0^t \frac{y(s)}{(t-s)^{-\gamma}} ds \right) \tag{19}$$

denotes the Riemann-Liouville fractional integral and

$$\frac{\partial^{1-\gamma} y(t)}{\partial t^{1-\gamma}} = {}_0D_t^{1-\gamma} y(t) \tag{20}$$

is the Riemann-Liouville fractional derivative defined in Eq. (11). The fractional differential operator $\mathcal{D}^{1-\gamma}$ is also related to the Caputo fractional differential operator via

$$\mathcal{D}^{1-\gamma} y(t) = {}_0^C D_t^{1-\gamma} y(t) + y(0^+)\delta(t). \tag{21}$$

In the remainder of this paper we consider Turing pattern formation in the fractional activator-inhibitor model system described by Eqs. (16) and (17) with zero-flux boundary conditions at both ends of the spatial domain of length L—i.e.,

$$\left.\frac{\partial n_j}{\partial x}\right|_{x=0} = 0, \qquad \left.\frac{\partial n_j}{\partial x}\right|_{x=L} = 0, \quad j=1,2. \tag{22}$$

III. LINEAR STABILITY ANALYSIS

In standard activator-inhibitor systems a Turing instability occurs if the homogeneous steady-state solution is linearly stable in the absence of diffusion but linearly unstable in the presence of diffusion. In the fractional activator-inhibitor system, Eqs. (16) and (17), the steady-state solution and the diffusion-free linear stability conditions are the same as in the standard ($\gamma=1$) activator-inhibitor system with the same reaction kinetics. Linear stability analysis in the fractional activator-inhibitor system can be facilitated by applying a temporal Laplace transform and a spatial Fourier transform. The transformed linearized perturbations are then given by [23]

$$\hat{\tilde{\Delta n}}_1(q,s) = \frac{(s+s^{1-\gamma_2}dq^2-\lambda a_{22})\tilde{\Delta n}_1(q,t=0) + \lambda a_{12}\tilde{\Delta n}_2(q,t=0)}{(s+s^{1-\gamma_1}q^2-\lambda a_{11})(s+s^{1-\gamma_2}dq^2-\lambda a_{22}) - \lambda^2 a_{12}a_{21}}, \tag{23}$$

$$\hat{\tilde{\Delta n}}_2(q,s) = \frac{(s+s^{1-\gamma_1}q^2-\lambda a_{11})\tilde{\Delta n}_2(q,t=0) + \lambda a_{21}\tilde{\Delta n}_1(q,t=0)}{(s+s^{1-\gamma_1}q^2-\lambda a_{11})(s+s^{1-\gamma_2}dq^2-\lambda a_{22}) - \lambda^2 a_{12}a_{21}}, \tag{24}$$

where s is the Laplace transform variable, q is the Fourier transform variable, a caret denotes a Laplace-transformed variable, and a tilde denotes a Fourier-transformed variable. The constants a_{ij} are defined by $a_{ij}=(\partial f_i/\partial n_j)|_{(n_1^\star,n_2^\star)}$ where $n_1^\star$ and $n_2^\star$ are the homogeneous steady state-concentrations.

In earlier work [23] we established Turing instabilities in the fractional activator-inhibitor system with Gierer-Meinhardt reaction kinetics and the special cases: (i) $\gamma_1=\frac{1}{2}$, $\gamma_2=1$, (ii) $\gamma_1=\gamma_2=\frac{1}{2}$, and (iii) $\gamma_1=1$, $\gamma_2=\frac{1}{2}$. We now consider the more general case defined by $\gamma_1=\gamma_2=\gamma$ and

$$1-\gamma = \frac{n}{m} \quad \text{where } n<m\in\mathbb{N}. \tag{25}$$

In this general case the canonical form for the Fourier-Laplace transforms of perturbations about the homogeneous steady state can be expressed as

$$\hat{\tilde{\Delta n}}(q,s) = \frac{\alpha(q)s + \beta(q)s^{n/m} + \gamma(q)}{\prod_{i=1}^{2m}(s^{1/m}-z_i)}, \tag{26}$$

where $\alpha(q)$, $\beta(q)$, and $\gamma(q)$ are real-valued functions of q and z_i are zeros of the polynomial

$$P_{2m} = (z^m + z^n q^2 - \lambda a_{11})(z^m + z^n dq^2 - \lambda a_{22}) - \lambda^2 a_{12}a_{21}. \tag{27}$$

The conditions for Turing instabilities can be found by investigating large-t asymptotic behavior from the inverse Laplace transform

$$\tilde{\Delta n}(q,t) = \frac{1}{2\pi i}\int_{c-i\infty}^{c+i\infty} \frac{\alpha(q)s + \beta(q)s^{n/m} + \gamma(q)}{\prod_{i=1}^{2m}(s^{1/m}-z_i)} e^{st} ds. \tag{28}$$

In Eq. (28), c denotes a real-valued constant to the right of all singularities in the complex plane.

This integral can be evaluated by considering a modified Bromwich contour Γ (see Fig. 1) with a branch cut from the branch point at $s=0$ and $s=re^{i\theta_p+2k\pi}$ with $-\pi<\theta_p\leqslant\pi$. It is straightforward to show that the contributions around the arcs vanish [23] so that

$$\tilde{\Delta n}(q,t) = \frac{1}{2\pi i}\left(\lim_{\epsilon\to\infty}\lim_{R\to\infty} \int_\Gamma \hat{\tilde{\Delta n}}(q,s)e^{st} ds - \lim_{\epsilon\to\infty}\lim_{R\to\infty} \int_{\vec{AB}} \hat{\tilde{\Delta n}}(q,s)e^{st} ds - \lim_{\epsilon\to\infty}\lim_{R\to\infty} \int_{\vec{CD}} \hat{\tilde{\Delta n}}(q,s)e^{st} ds \right). \tag{29}$$

It is clear from the Cauchy residue theorem that exponentially unstable Fourier modes (wave numbers) will arise from the poles in Eq. (26)—i.e., from the zeros of the polynomial,

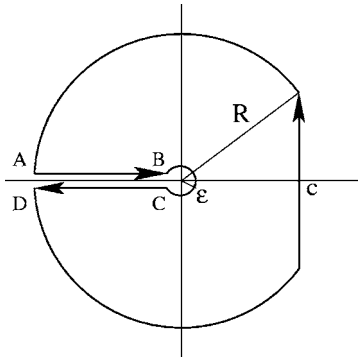

FIG. 1. Modified Bromwich contour for the inverse Laplace transform.

Eq. (27). In particular if $z_k(q)$ is a zero of this polynomial and $\mathrm{Re}[z_k^m(q)]>0$ for some wave numbers $q\neq 0$, then these wave numbers will be linearly unstable. The homogeneous steady state is linearly stable in the absence of diffusion if $\mathrm{Re}[z_k(q)]=0$. It is not possible to obtain algebraic expressions for the zeros of Eq. (27); however, for prescribed values of the system parameters m, n, $a_{i,j}$, d, and λ, these zeros can be found numerically over a range of q and a minimum value of d can be determined for which there exists a zero $z_k(q)$ such that $\mathrm{Re}[z_k^m(q)]\geqslant 0$. In the linear theory a spatial pattern might be expected to emerge from the Turing instability if only a finite set of wave numbers is unstable or if one excited mode is dominant. The range of wave numbers that are unstable and the most unstable wave number in the linear theory can be found by fixing the parameters m, n, $a_{i,j}$, d, and λ and finding the zeros, $z_k(q)$, of Eq. (27) numerically over a range of q. At each q value we can determine the maximum value of $\mathrm{Re}[z_k^m(q)]$ from this set of zeros. Then we plot this maximum value as a function of q. The range is identified as the set of q values over which the maximum is greater than zero and the most unstable wave number (maximally excited mode) is the q value where this curve has a maximum.

The results of the linear stability analysis of the homogeneous steady-state solution for the fractional activator-inhibitor systems with Gierer-Meinhardt reaction kinetics and with Brusselator reaction kinetics are presented in the next two sections.

A. Gierer-Meinhardt reaction kinetics

The Gierer-Meinhardt reaction kinetics is defined by [34]

$$f_1(n_1,n_2)=1-n_1+3\frac{n_1^2}{n_2}, \tag{30}$$

$$f_2(n_1,n_2)=n_1^2-n_2. \tag{31}$$

The fractional activator-inhibitor system defined by Eqs. (16), (17), and (22) and the above reaction kinetics has a homogeneous steady state of $n_1^*=4$ and $n_2^*=16$. Standard linear stability analysis [9,23] reveals that in the case of standard diffusion ($\gamma_1=\gamma_2=1$) nonhomogeneous steady states can occur if the value of d exceeds the critical value

$$d^\star=10+4\sqrt{6}\simeq 19.79. \tag{32}$$

For $d>d^\star$ the range of excited Fourier modes q is given by [see Eq. (6)]

$$\frac{d-2-\sqrt{d^2-20d+4}}{4d}\leqslant q^2\leqslant\frac{d-2+\sqrt{d^2-20d+4}}{4d}. \tag{33}$$

For $d<d^\star$ initial perturbations about the steady state decay to zero for all wave numbers and no pattern results.

In Table I we have listed the critical value of $d^\star$ over a range of γ based on the linear stability analysis of the fractional activator-inhibitor system with Gierer-Meinhardt reaction kinetics. We have also identified the maximally excited mode and the range of excited modes based on the linear stability analysis over a range of γ values for a given value of $d>d^*$ for each γ.

The following pattern of behavior is consistent with the results in this table: (i) The critical value of d^* decreases monotonically with increasing $1-\gamma$—i.e., as the diffusion

TABLE I. The critical values of $d^\star$ for different γ values as predicted from linear stability analysis for the fractional Gierer-Meinhardt model. The maximally excited Fourier mode and the range of excited Fourier modes are also listed for different γ values with $d>d^\star$. In the case $\gamma=0.8$ there were two dominant modes resulting from the linear stability analysis.

γ	$d^\star$	d	Max mode	Mode range
0.1	3.102	4.0	1.6556	$q\geqslant 1.0937$
0.2	4.672	7.0	1.1470	$q\geqslant 0.7277$
0.3	6.701	9.0	1.0949	$q\geqslant 0.7378$
0.4	9.088	12.0	0.9655	$q\geqslant 0.6681$
0.5	11.657	14.0	0.9272	$q\geqslant 0.6866$
0.6	14.190	17.0	0.8117	$q\geqslant 0.6149$
0.7	16.459	19.0	0.7334	$q\geqslant 0.5799$
0.8	18.253	21.0	0.6384 (0.7184)	$q\geqslant 0.5161$
0.9	19.402	22.0	0.5578	$q\geqslant 0.4587$
1.0	19.798	22.0	0.4632	$0.3854\leqslant q\leqslant 0.5532$

TABLE II. The critical values of $d^\star$ for different γ values as predicted from linear stability analysis for the fractional Brusselator model. The maximally excited Fourier mode and the range of excited Fourier modes are also listed for different γ values with $d > d^\star$.

γ	$d^\star$	d	Max mode	Mode range
0.1	5.462	7.0	2.0396	$q \geqslant 1.4035$
0.2	7.351	9.0	1.8527	$q \geqslant 1.3187$
0.3	9.638	11.0	1.7849	$q \geqslant 1.3287$
0.4	12.218	14.0	1.4648	$q \geqslant 1.1116$
0.5	14.928	17.0	1.2530	$q \geqslant 0.9712$
0.6	17.561	20.0	1.0800	$q \geqslant 0.8505$
0.7	19.898	22.0	0.9764	$q \geqslant 0.7959$
0.8	21.736	23.0	0.8946	$q \geqslant 0.7686$
0.9	22.910	24.0	0.7974	$q \geqslant 0.6810$
1.0	23.314	25.0	0.6360	$0.5403 \leqslant q \leqslant 0.7403$

becomes more subdiffusive. (ii) The maximally excited-mode wave number increases as the fractional derivative exponent $1-\gamma$ increases; i.e., the wavelength of the maximally excited mode decreases as the subdiffusion becomes more anomalous. (iii) The minimum wave number cutoff for the range of excited modes also increases as the fractional derivative exponent $1-\gamma$ increases. (iv) There is no upper wave number cutoff for excited modes for $0 < 1-\gamma < 1$.

B. Brusselator reaction kinetics

The Brusselator reaction kinetics considered in this paper is defined by [35]

$$f_1(n_1,n_2) = 2 - 3n_1 + n_1^2 n_2, \tag{34}$$

$$f_2(n_1,n_2) = 2n_1 - n_1^2 n_2. \tag{35}$$

The homogeneous steady-state solution is given by $n_1^*=2$ and $n_2^*=1$. The critical value of d for a Turing instability, which follows from Eq. (5), is thus given by

$$d^\star = 12 + 8\sqrt{2} \approx 23.31 \tag{36}$$

and the range of excited Fourier modes from Eq. (6) is

$$\frac{d-4-\sqrt{d^2-24d+16}}{2d} \leqslant q^2 \leqslant \frac{d-4+\sqrt{d^2-24d+16}}{2d}. \tag{37}$$

In Table II we have listed the critical value of d^* over a range of γ based on the linear stability analysis of the fractional activator-inhibitor system with Brusselator reaction kinetics. We have also identified the maximally excited mode and the range of excited modes based on the linear stability analysis over a range of γ values with $d > d^*$ for each γ. The overall pattern of behavior is similar to that found for the fractional Gierer-Meinhardt model.

The results of the linear stability analysis in this section for fractional activator-inhibitor systems with the same subdiffusion exponent γ can be summarized as follows: The critical value of the diffusion coefficient ratio d^* for the onset of a Turing instability decreases monotonically as the subdiffusion becomes more anomalous (the scaling exponent γ is further from unity). Modes of arbitrarily small wavelength become excited for $d > d^*$. The wavelength of the maximally excited mode becomes shorter as the subdiffusion becomes more anomalous and the upper threshold wavelength of excited modes decreases as the subdiffusion becomes more anomalous.

IV. NUMERICAL SIMULATIONS

We have carried out extensive numerical simulations of the fractional activator-inhibitor system for both Gierer-Meinhardt and Brusselator reaction kinetics and for a range of system parameters. The purpose of these numerical simulations is to test the linear stability analysis as a predictor of Turing pattern formation in nonlinear fractional activator-inhibitor systems as well as to investigate the nature of patterns formed in these systems. The numerical scheme that we have employed is an implicit finite-difference scheme, and we have reported on the accuracy and stability of this method elsewhere [46]. Further details of the implementation of our scheme are provided in the Appendix.

We have carried out numerical simulations of the fractional activator-inhibitor model with both Gierer-Meinhardt reaction kinetics and with Brusselator reaction kinetics over a range of system parameters and with initial conditions perturbed about the homogeneous steady-state solution—i.e., $n_j(x,0) = n_j^* + \delta n_j(x,0)$. Three different types of perturbation have been considered: (i) random, $\delta n_j(x,0) = \epsilon r_j(x)$ where $r_j(x)$ is a uniform random function on the interval $[-1,1]$; (ii) long-wavelength sinusoidal, $\delta n_j(x,0) = \epsilon \sin(qx)$, with $q = 0.4$ (Gierer-Meinhardt) or $q = 0.5$ (Brusselator); (iii) short-wavelength sinusoidal, $\delta n_j(x,0) = \epsilon \sin(qx)$, with $q = 5$ (both Gierer-Meinhardt and Brusselator). In each case we have set $\epsilon = 10^{-2}$.

A. Turing instabilities

In the first instance we have used our simulations to test whether or not the Turing instability bifurcation curves from

linear stability analysis delimit stable and unstable regions in the anomalous diffusion parameter space in the nonlinear fractional activator-inhibitor systems.

To determine the temporal growth of the initial perturbation we ran the simulation for 1000 units of time with a time step $\Delta t=0.1$. The length of the region was taken to be $L=100$ with $N=128$ grid points in the simulation. Thus the spatial grid size is $\Delta x=L/N=0.78$. The numerical simulations are used to find the concentrations $n_j(x,t)$ at each spatial grid point $x=i\Delta x$ and at each discrete time step $t=(k-1)\Delta t$. In the following we use the notation

$$n_{j,i}^k = n_j(i\Delta x,(k-1)\Delta t). \tag{38}$$

At each time step $k\in[1,1000]$, the maximum absolute deviation from the homogeneous steady state was calculated for both n_1 and n_2;

$$A_1^*(t_k) = \max_{1\leqslant i\leqslant N} |n_{1,i}^k - n_1^\star|, \tag{39}$$

$$A_2^*(t_k) = \max_{1\leqslant i\leqslant N} |n_{2,i}^k - n_2^\star|. \tag{40}$$

The resultant spatial patterns appeared to be stationary or quasistationary after a typical transient time of about 500 model time units. A crude numerical estimate of the critical value of d separating stable and unstable behavior was found by using randomly perturbed initial conditions and measuring

$$g_j = \frac{\sum_{t_k\in[500,1000]} A_j^*(t_k)}{\sum_{t_k\in[0,500]} A_j^*(t_k)}, \quad j=1,2, \tag{41}$$

over a range of d, and then identifying the minimum value d for which

$$\min_{j=1,2} g_j \geqslant 1.$$

For d values below this threshold we have a stable homogeneous steady state and for d values above this threshold we have growth of perturbations about the steady state for both n_1 and n_2.

Comparisons between (i) our numerical estimates of the threshold value of d separating stable and unstable regions, and (ii) the critical values of d^* for a Turing instability from the linear stability analysis for the fractional Gierer-Meinhardt system and the fractional Brusselator system are shown in Figs. 2 and 3, respectively. It is clear from these comparisons, shown over a range of γ, that the Turing instability conditions determined in Sec. III do delimit stable and unstable regions in the anomalous diffusion parameter space for nonlinear fractional activator-inhibitor systems. It is also worthwhile reemphasizing the overall trends shown in these figures: namely, that Turing patterns can occur for lower values of the diffusion constant d as the (sub)diffusion becomes more anomalous (decreasing γ).

B. Spatiotemporal Turing patterns $\gamma_1=\gamma_2=\gamma$

In this subsection we describe our numerical results on the maximally excited wave numbers in fractional activator-inhibitor systems (with Gierer-Meinhardt reaction kinetics and with Brusselator reaction kinetics) for a range of γ and $d>d^\star$. The anomalous diffusion exponent is taken to be the same for both the activator and inhibitor in these simulations—i.e., $\gamma_1=\gamma_2=\gamma$. The results are based on simulations over 1500 units of time with a step size of $\Delta t=0.1$ and a spatial grid of 256 points with $L=100$. We have carried out simulations for a range of $\gamma=0.1,0.2,0.3,\ldots,0.9,1.0$ and for the random perturbations, short-wavelength perturbations, and long-wavelength perturbations of the steady state.

The dominant excited Fourier modes $q=(2\pi/L)k$ were determined from the positions k of the peaks in the spatial power spectrum for n_1 and n_2 at the end of the simulation, $t=1500$. Explicitly the power spectrum is defined by

$$P_j(k) = \frac{1}{N} z_j(k) z_j^*(k),$$

where

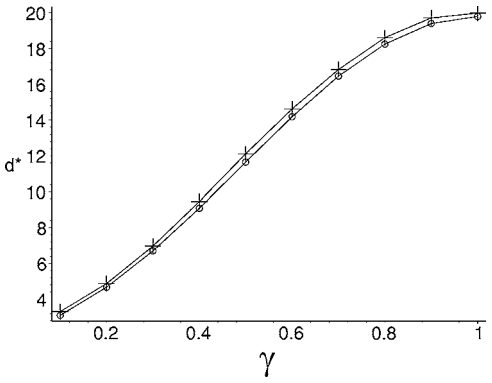

FIG. 2. Estimates of the critical value of $d^\star$ from the linear stability analysis (○) compared with estimates from the growth of modes in numerical simulations (+) for the fractional activator-inhibitor system with Gierer-Meinhardt reaction kinetics and the same value γ for the activator and inhibitor diffusion exponents. The quantities plotted are dimensionless.

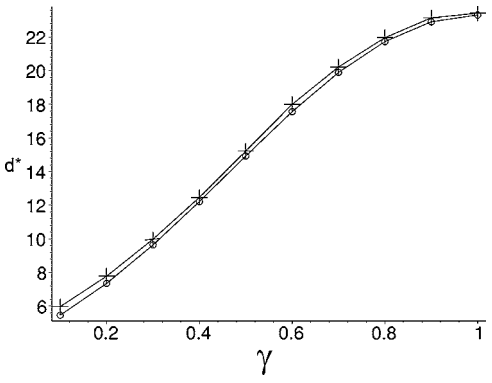

FIG. 3. Estimates of the critical value of $d^\star$ from the linear stability analysis (○) compared with estimates from the growth of modes in numerical simulations (+) for the fractional activator-inhibitor system with Brusselator reaction kinetics and the same value γ for the activator and inhibitor diffusion exponents. The quantities plotted are dimensionless.

TABLE III. The dominant (maximum k) Fourier wave numbers determined by linear stability analysis and the positions of peaks in the power spectra from numerical simulations. Results here are shown with Gierer-Meinhardt reaction kinetics. The asterisk is used to identify the k value corresponding to the largest peak in the power spectrum.

			Power spectra peaks	
γ	d	Maximum k	n_1	n_2
0.2	7.0	18.5	16, 17, 34, 37*	16, 18, 19, 34*
0.4	12.0	15.5	15*, 29, 31	14, 15*, 29, 30, 31
0.5	14.0	15.0	13*, 28, 29	13*, 29
0.6	17.0	13.0	14*, 28	14*, 28
0.7	19.0	11.5	12*, 24	11*, 13, 24
0.8	21.0	10.0, 11.5	11*	11*
0.9	22.0	9.0	9*	9*
1.0	22.0	7.5	7, 8*	7, 8*

$$z_j(k) = \sum_{n=1}^{N} n_j(n\Delta x, 1500) x_n e^{-2\pi i(k-1)(n-1)/N}, \quad k = 1,2,\ldots,N,$$

was computed using a fast Fourier transform. The spatial grid size limits the resolution of Fourier modes to $\pm 2\pi/100 \approx \pm 0.062$.

Partial results from our simulations are summarized in Tables III and IV for Gierer-Meinhardt reaction kinetics and Brusselator reaction kinetics, respectively, using random perturbations about the homogeneous steady state as initial conditions. In these tables we have listed (i) the $d > d^\star$ values used in the numerical simulations, (ii) the values of the nearest maximally excited wave numbers k corresponding to the maximally excited Fourier modes q in the linear stability analysis (see Tables I and II), and (iii) the values of the wave numbers k corresponding to peaks in the power spectra (for both n_1 and n_2), the largest of these peaks is highlighted using an asterisk.

The position of the largest peak in the power spectrum does not always match the maximally excited mode as determined by the linear stability analysis but there is generally a peak in the power spectra at a k value close to that of the maximally excited mode. This provides evidence that linear stability analysis is not only a reliable predictor of the onset of Turing instabilities (critical d values) but it also provides a useful description (dominant modes) of the nature of the Turing patterns in nonlinear fractional activator-inhibitor systems. The linear stability analysis is a better indicator of the dominant excited mode when γ is closer to unity (standard diffusion) but this may be because the numerical simulations take longer to reach the quasistationary regime for smaller γ values. The results with sinusoidally perturbed initial conditions show the same overall pattern of behavior as those with randomly perturbed initial conditions and so the details have not been tabulated in this paper [47].

Further results from our numerical simulations are shown in Figs. 4 and 5. These figures show full surface profiles and surface density plots for the concentrations of the activator with randomly perturbed initial conditions. The behavior of the inhibitor (not shown here [47]) is similar to that of the activator. In the surface density plots $n_1(x,t) \geqslant n_1^\star$ is shown as black and $n_1(x,t) < n_1^\star$ as white. Figure 4 shows results for the fractional Gierer-Meinhardt model, and Fig. 5 shows results for the fractional Brusselator model.

The following observations summarize the principal features in our simulations of perturbed fractional activator-inhibitor systems with equal anomalous diffusion in both the activator and the inhibitor: (i) The concentrations of the activator and inhibitor both fluctuate (more or less to the same degree) about the homogeneous steady-state values. (ii) A spatiotemporal pattern develops on or before about 500 model time units. (iii) The surface profiles become more spatially rough as γ decreases. (iv) The surface profiles become less stationary in time as γ decreases. [The alternating bands of black and white along the time axis in Fig. 4(b) are characteristic of standing wave patterns.]

In order to further explore the robustness of the above results we have carried out additional simulations using different (sinusoidally perturbed) initial conditions. Surface

TABLE IV. The dominant (maximum k) Fourier wave numbers determined by linear stability analysis and the positions of peaks in the power spectra from numerical simulations. Results here are shown with Brusselator reaction kinetics. The asterisk is used to identify the k value corresponding to the largest peak in the power spectrum.

			Power spectra peaks	
γ	d	Maximum k	n_1	n_2
0.2	9.0	29.5	30, 32*, 62	30*, 32, 62
0.4	14.0	23.5	24, 25*, 27, 55	25*, 27
0.5	17.0	20.0	20*, 38, 39	20*, 38, 39
0.6	20.0	17.0	18, 19*, 37	18, 19*, 37
0.7	22.0	15.5	15, 16*, 31	15, 16*, 31
0.8	23.0	14.0, 14.5	14, 15*, 29	14, 15*, 29
0.9	24.0	12.5	13*	13*
1.0	25.0	10.0	10, 11*	10, 11*

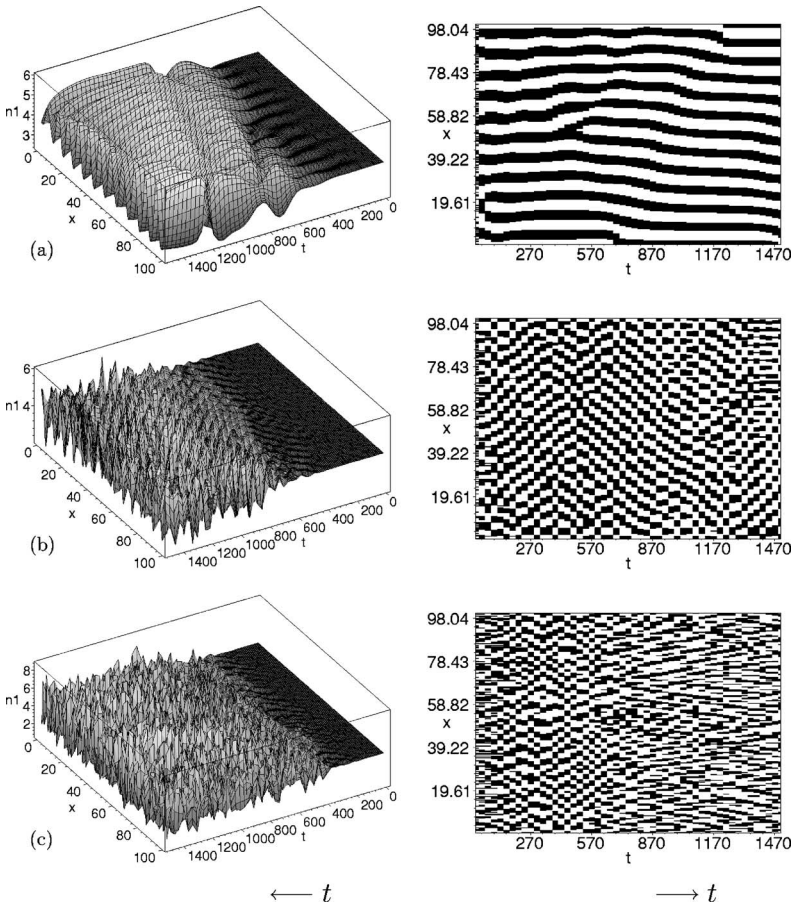

FIG. 4. Surface profiles and surface density plots for $n_1(x,t)$ in the fractional Gierer-Meinhardt model with randomly perturbed initial conditions: (a) $\gamma=0.8$, $d=21$; (b) $\gamma=0.5$, $d=14$; (c) $\gamma=0.2$, $d=7$. The quantities plotted are dimensionless.

density plots are shown in Fig. 6 for the fractional Brusselator model using long-wavelength sinusoidal perturbations (left) and short-wavelength sinusoidal perturbations (right). The persistence of the memory effect is greater for lower values of γ but in all cases there appears to be no memory of the initial conditions after 500 model time units. The patterns after this time are essentially the same for long-wavelength, short-wavelength, and random initial pertubations.

An interesting question is whether the surfaces that we have described here as rough possess self-affine scaling properties characteristic of fractional Brownian functions [48–51]. Preliminary measurements of surface roughness that we have carried out [27] are consistent with self-affine scaling with a Hurst exponent H that decreases essentially monotonically in the range between $H=1$ (smooth curve) and $H=1/2$ (ordinary Brownian function) as γ varies from unity (normal diffusion) to zero. However, these results, which typically are based on log-log plots spanning less than an order of magnitude in the spatial grid size Δx, will require confirmation from simulations with greater spatial resolution.

C. Stationary Turing patterns $\gamma_1=0.5, \gamma_2=1.0$

In a previous paper [23] we carried out linear stability analysis of the homogeneous steady state for fractional activator-inhibitor systems with standard diffusion in the inhibitor ($\gamma_2=1.0$) but anomalous subdiffusion in the activator ($\gamma_1=0.5$). On the basis of this analysis we speculated that Turing-instability-induced pattern formation might occur in such systems for any nonzero d. In order to test this speculation we have carried out numerical simulations of the fractional activator-inhibitor model with standard diffusion in the inhibitor and anomalous subdiffusion in the activator over a range of parameters with both Gierer-Meinhardt and with Brusselator reaction kinetics. Sample results are shown in the plots in Figs. 7–9. Figures 7 and 8 show surface profiles and density plots for the activator in the fractional Gierer-Meinhardt system and the fractional Brusselator system, respectively. Figure 9 shows example surface profiles for the inhibitor in fractional activator-inhibitor systems with fractional diffusion in the activator but standard diffusion in the inhibitor. Standard density plots corresponding to these profiles are either all white or all black. In Fig. 10 we have plotted the characteristic wavelength of the stationary pattern (defined as the length of the domain divided by the number of peaks in the stationary pattern) as a function of the diffusion ratio d.

The following features are common to the simulations that we carried out with anomalous subdiffusion in the activator but standard diffusion in the inhibitor: (i) The activator and inhibitor do not exhibit similar fluctuations about the homogeneous steady-state solution. (ii) Pattern formation occurs for values of d below the critical $d^\star$ for pattern formation in the same model systems but with standard diffusion ($\gamma=1$) or fractional diffusion ($\gamma=1/2$) in both the activator and the inhibitor. (iii) The patterns are stationary. (iv) The patterns are not rough. (v) The wavelength of the patterns increases as d increases.

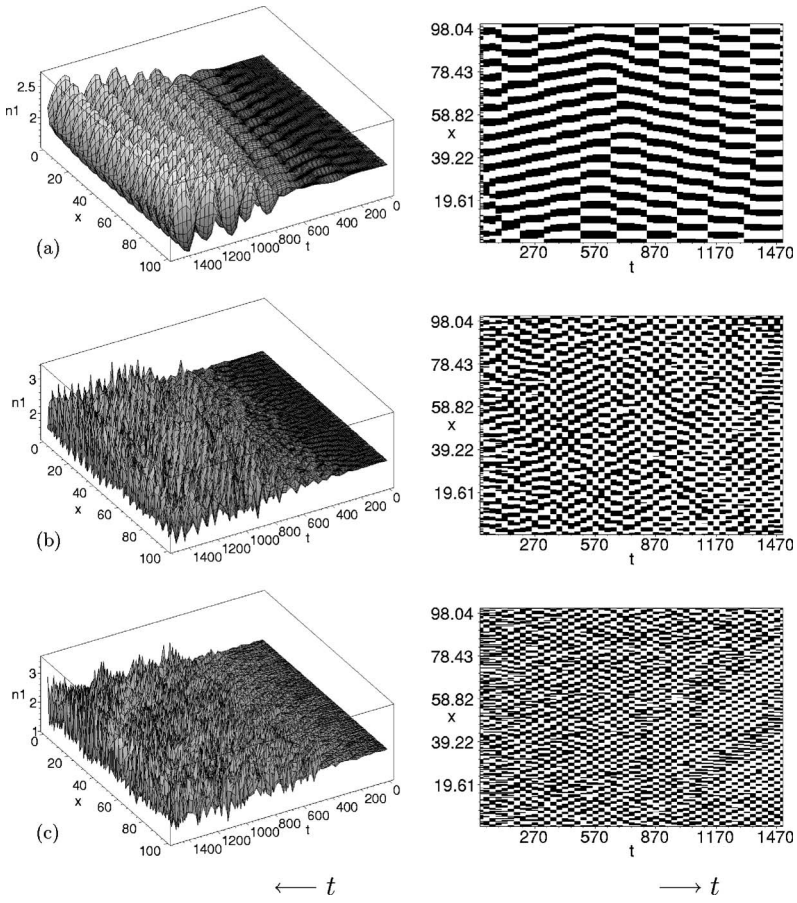

FIG. 5. Surface profiles and surface density plots for $n_1(x,t)$ in the fractional Brusselator model with randomly perturbed initial conditions: (a) $\gamma=0.8$, $d=23$; (b) $\gamma=0.5$, $d=17$; (c) $\gamma=0.2$, $d=9$. The quantities plotted are dimensionless.

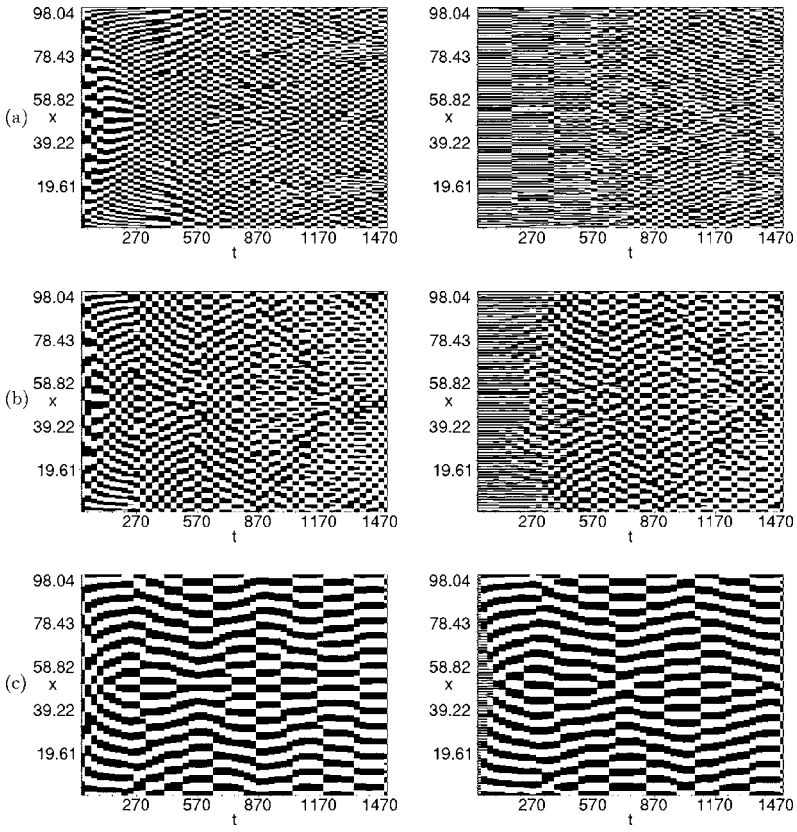

FIG. 6. Surface density plots for the activator, $n_1(x,t)$, in the fractional Brusselator model with long-wavelength (left column) and short-wavelength (right column) sinusoidally perturbed initial conditions: (a) $\gamma=0.2$, $d=9$; (b) $\gamma=0.5$, $d=17$; (c) $\gamma=0.8$, $d=23$. The quantities plotted are dimensionless.

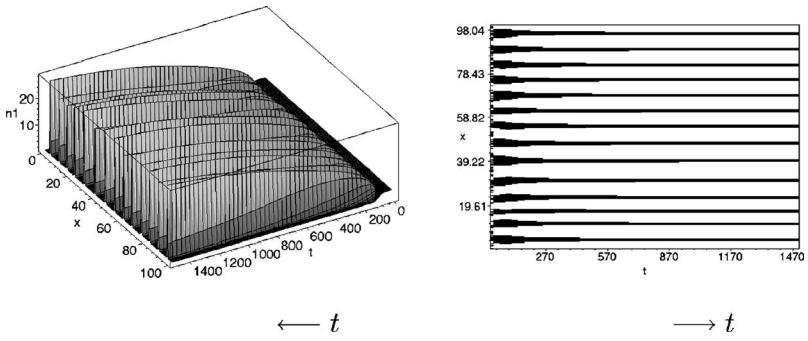

$\longleftarrow t$ $\longrightarrow t$

FIG. 7. Surface profile and surface density plot for the activator, $n_1(x,t)$, in the fractional Gierer Meinhardt model with randomly perturbed initial conditions and diffusion parameters $\gamma_1 = 0.5$, $\gamma_2 = 1.0$, and $d = 8$. The quantities plotted are dimensionless.

V. DISCUSSION

In this paper we have carried out algebraic and numerical analysis of fractional activator-inhibitor systems with Gierer-Meinhardt and with Brusselator reaction kinetics. We have considered cases with equal anomalous (sub)diffusion in both activator and inhibitor variables as well as cases with anomalous (sub)diffusion in the activator but standard diffusion in the inhibitor. The anomalous subdiffusion is characterized by the two variables d (a diffusion constant) and γ (a diffusion scaling exponent) through the relation [52]

$$\langle r^2(t)\rangle = \frac{2d}{\Gamma(1+\gamma)} t^{\gamma}, \tag{42}$$

where $\langle r^2(t)\rangle$ is the mean-square distance traveled by a diffusing particle in time t. In the case of standard diffusion, $\gamma = 1$, and as γ is reduced from 1 to 0, the (sub)diffusion becomes more anomalous.

Our results provide clear evidence for the following: (i) Linear stability analysis of homogeneous steady-state solutions provides a reliable predictor of the onset and nature of pattern formation in fractional activator-inhibitor systems. (ii) Turing instabilities occur for successively lower values of the critical diffusion constant $d^{\star}$ as the (sub)diffusion becomes more anomalous. (iii) Spatiotemporal patterning occurs in fractional activator-inhibitor systems when the diffusion is equally anomalous in both the activator and inhibitor. The patterning is similar in both the activator and inhibitor in these systems. The surface profiles are increasingly rough as the (sub)diffusion becomes more anomalous. (iv) Stationary Turing patterns occur in fractional activator-inhibitor systems when the diffusion is anomalous subdiffusion in the activator but standard diffusion in the inhibitor. The patterning is different in the activator and inhibitor in these systems and it is not rough.

In standard activator-inhibitor systems it is well known that a necessary condition for pattern formation is that the inhibitor concentration diffuses faster than the activator concentration (see, e.g., [9]). Thus in time t we would expect the mean-square displacement of the inhibitor $\langle r_2^2(t)\rangle$ to be greater than that of the activator $\langle r_1^2(t)\rangle$. Allowing for anomalous diffusion as in Eq. (42) this yields the result that

$$d = \frac{d_2}{d_1} > \frac{t^{\gamma_1}\Gamma(1+\gamma_2)}{t^{\gamma_2}\Gamma(1+\gamma_1)}. \tag{43}$$

so that if $\gamma_1 < \gamma_2$, then after a sufficiently long time this condition will always be satisfied. The results of our studies are consistent with this general principle.

The results of this paper provide theoretical support for fractional activator-inhibitor systems as viable models for Turing pattern formation in activator-inhibitor systems with anomalous subdiffusion in one or both of the chemically reacting species. In experimental studies of Turing pattern formation in activator-inhibitor systems it has been argued that the diffusion rate of the activator is effectively reduced by the reaction medium (a gel containing a colour indicator). It would be useful to have experiments that directly test for anomalous subdiffusion of the activator in the reaction medium in the absence of the inhibitor. Some practical considerations on how this might be done are described in [52].

ACKNOWLEDGMENTS

We greatfully acknowledge discussions with Prof. Dr. Igor M. Sokolov. The work was supported by an ARC Discovery Grant funded by the Australian Commonwealth Government.

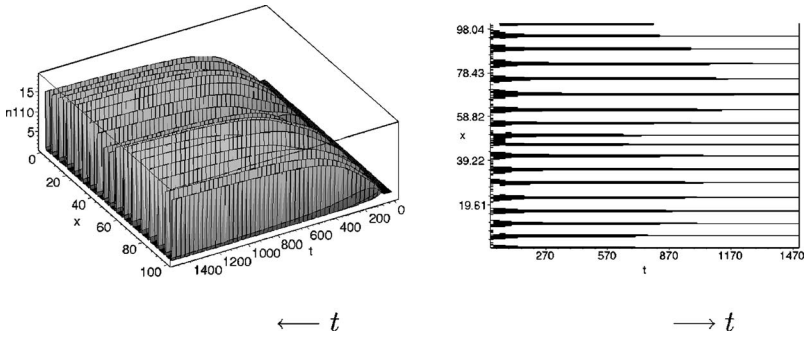

$\longleftarrow t$ $\longrightarrow t$

FIG. 8. Surface profile and surface density plot for the activator, $n_1(x,t)$, in the fractional Brusselator model with randomly perturbed initial conditions and diffusion parameters $\gamma_1 = 0.5$, $\gamma_2 = 1.0$, and $d = 10$. The quantities plotted are dimensionless.

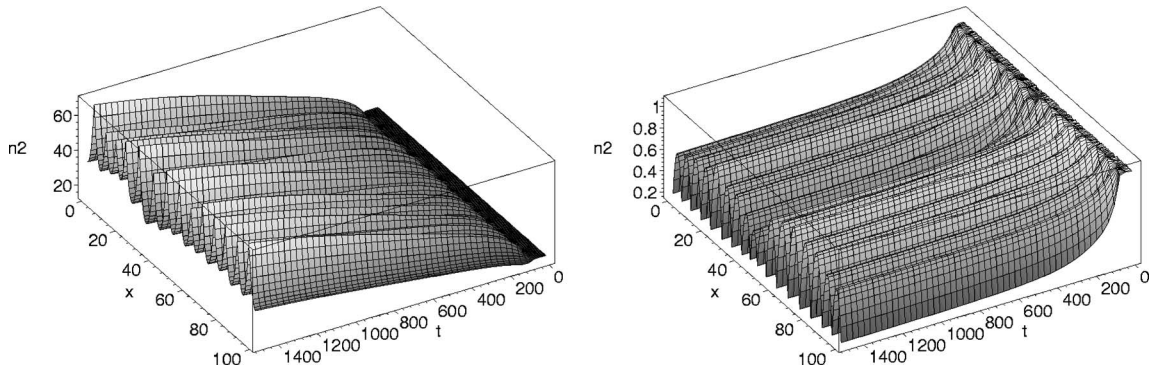

FIG. 9. Surface profiles for the inhibitor, $n_2(x,t)$, in the fractional Gierer-Meinhardt model (left) and the fractional Brusselator model (right) with randomly perturbed initial conditions and with diffusion parameters $\gamma_1=0.5$, $\gamma_2=1.0$, and $d=8.0$ (Gierer-Meinhardt) or $d=10.0$ (Brusselator). The quantities plotted are dimensionless.

APPENDIX: IMPLICIT NUMERICAL SCHEME FOR FRACTIONAL ACTIVATOR-INHIBITOR SYSTEMS

The model equations (16) and (17) were discretized using finite differences with a backward Euler time step for the time derivative and a centered difference approximation for the spatial derivative. The fractional derivative of order $1-\gamma$ with respect to time at $t=t_{k+1}$ was approximated using the L1 scheme [53]

$$\frac{d^{1-\gamma}y}{dt^{1-\gamma}} \approx \frac{\Delta t^{\gamma-1}}{\Gamma(1+\gamma)} \times \left\{ \frac{\gamma y(0)}{k^{1-\gamma}} + \sum_{l=1}^{k} [y(t_{l+1}) - y(t_l)][(k-l+1)^{\gamma} - (k-l)^{\gamma}] \right\},$$

where Δt is the step length in time and $\Gamma(x)$ is the gamma function. We retain the full evaluation of the sum in the L1 scheme for the computation of the fractional derivative. Our implicit method reduces to the solution of a set of $2N$ nonlinear equations in $2N$ unknowns to be solved at each step. The equations are

$$n_{1,i}^{k+1} - n_{1,i}^{k} - \Delta t f_1(n_{1,i}^{k+1}, n_{2,i}^{k+1}) - \delta_1 \frac{\gamma_1}{k^{1-\gamma_1}} \nabla n_{1,i}^{1} - \delta_1 \sum_{l=1}^{k} (\nabla n_{1,i}^{l+1} - \nabla n_{1,i}^{l})[(k-l+1)^{\gamma_1} - (k-l)^{\gamma_1}] = 0, \quad \text{(A1)}$$

$$n_{2,i}^{k+1} - n_{2,i}^{k} - \Delta t f_2(n_{1,i}^{k+1}, n_{2,i}^{k+1}) - \delta_2 \frac{\gamma_2}{k^{1-\gamma_2}} \nabla n_{2,i}^{1} - \delta_2 \sum_{l=1}^{k} (\nabla n_{2,i}^{l+1} - \nabla n_{2,i}^{l})[(k-l+1)^{\gamma_2} - (k-l)^{\gamma_2}] = 0, \quad \text{(A2)}$$

where $n_{j,i}^{k}=n_j(i\Delta x,(k-1)\Delta t)$,

$$\delta_1 = \frac{\Delta t^{\gamma_1}}{\Delta x^2 \Gamma(1+\gamma_1)}, \quad \delta_2 = d\frac{\Delta t^{\gamma_2}}{\Delta x^2 \Gamma(1+\gamma_2)}$$

and

$$\nabla n_{j,i}^{k} = n_{j,i+1}^{k} - 2n_{j,i}^{k} + n_{j,i-1}^{k}.$$

The above nonlinear equations are solved at each iteration using the Newton-Raphson numerical solution technique. The sum in the finite difference equations, Eqs. (A1) and (A2), can be evaluated once at each time step rather than at each iteration per time step since only the kth term $\nabla n_{j,i}^{k}$ of the sum involves the unknown variables; the rest of the sum remains constant per iteration for a given time step. To realize these savings we have rewritten the finite-difference equations as

$$n_{j,i}^{k+1} - \Delta t f_j(n_{1,i}^{k+1}, n_{2,i}^{k+1}) - \delta_j \nabla n_{j,i}^{k+1} = n_{j,i}^{k} + \left\{ \nabla n_{j,i}^{1} \omega_j^{k} + \sum_{l=2}^{k} \beta_{k-l+2} \nabla n_{j,i}^{l} \right\},$$

where $i=1,2,\ldots,N$ and $j=1,2$. The weights of the fractional derivative are given by

$$\omega_j^{k} = \frac{\gamma_j}{k^{1-\gamma_j}} - [k^{\gamma_j} - (k-1)^{\gamma_j}]$$

and

$$\beta_s = s^{\gamma_j} - 2(s-1)^{\gamma_j} + (s-2)^{\gamma_j} s = 2,3,\ldots,k.$$

The "constant" terms of the sum are now given on the right of these equations. The above system of $2N$ nonlinear equations was solved using the Newton-Raphson method [54]

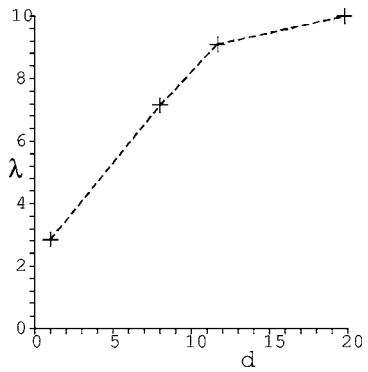

FIG. 10. Characteristic wavelength versus diffusion ratio for stationary patterns in the fractional Gierer-Meinhardt system with random initial conditions and with $\gamma_1=0.5$ and $\gamma_2=1.0$. The quantities plotted are dimensionless.

and at each iteration the system of linear equations

$$\mathbf{J}(\underset{\sim}{x}^i)\,\delta\underset{\sim}{x} = -\underset{\sim}{f}(\underset{\sim}{x}^i)$$

was solved to find the correction. A modified Crout algorithm was used to solve this system of equations. The Crout algorithm was made more efficient by taking into account the block structure of the Jacobi matrix

$$\mathbf{J} = \begin{bmatrix} \mathbf{T}_1 & \mathbf{D}_1 \\ \mathbf{D}_2 & \mathbf{T}_2 \end{bmatrix},$$

where $\mathbf{T}_j$ and $\mathbf{D}_j$ are $N \times N$ tridiagonal and diagonal matrices, respectively. The decomposed Jacobi matrix can be shown to take the form

$$\mathbf{J}^* = \begin{bmatrix} \mathbf{T} & \mathbf{L} \\ \mathbf{U} & \mathbf{S} \end{bmatrix},$$

where $\mathbf{L}$, $\mathbf{U}$, and $\mathbf{S}$ are $N \times N$ lower triangular, upper triangular, and square matrices, respectively. A significant amount of computation can be saved by only computing elements we know to be nonzero. Some idea of the savings achieved can be obtained by noting that $4N^2$ elements are evaluated in the full method whereas only $2N^2+2N-1$ elements need to be evaluated in the modified method (the elements on the upper diagonal of T_1 and on the diagonal of D_1 remain unchanged and hence do not need to be evaluated). In terms of computation, the full Crout method requires $N(8N^2+30N-11)/3$ operations while the modified method requires only $(4N^3+21N^2+17N-6)/3$ operations, a saving of about 50% for $N=128$.

[1] A. M. Turing, Philos. Trans. R. Soc. London, Ser. B **327**, 37 (1952).
[2] K. Kondo and R. Asai, Nature (London) **376**, 765 (1995).
[3] P. K. Maini, K. J. Painter, and H. N. P. Chau, J. Chem. Soc., Faraday Trans. **93**, 3601 (1997).
[4] V. Castets, E. Dulos, J. Boissonade, and P. De Kepper, Phys. Rev. Lett. **64**, 2953 (1990).
[5] P. Liang, Phys. Rev. Lett. **75**, 1863 (1995).
[6] Y. Astrov, E. Ammelt, S. Teperick, and H. G. Purwins, Phys. Lett. A **211**, 184 (1996).
[7] F. T. Arecchi, S. Boccaletti, and P.-L. Ramazza, Phys. Rep. **318**, 1 (1999).
[8] K. Staliunas and V. J. Sánchez-Morcillo, Opt. Commun. **177**, 389 (2000).
[9] J. D. Murray, *Mathematical Biology II: Spatial Models and Biomedical Applications*, 3rd ed. (Springer-Verlag, New York, 2003).
[10] T. Shin, D. Kraemer, J. Pryor, L. Liu, J. Rugila, L. Howe, S. Buck, K. Murphy, L. Lyons, and M. Westhusin, Nature (London) **415**, 859 (2002).
[11] G. Nicolis, Faraday Discuss. **120**, 1 (2001).
[12] D. ben Avraham and S. Havlin, *Diffusion and Reactions in Fractals and Disordered Systems* (Cambridge University Press, Cambridge, England, 2000).
[13] J.-P. Voroney, A. T. Lawniczak, and R. Kapral, Physica D **99**, 303 (1996).
[14] R. N. Ghosh and W. W. Webb, Biophys. J. **68**, 766 (1994).
[15] T. J. Feder, I. Brust-Mascher, J. P. Slattery, B. Baird, and W. W. Webb, Biophys. J. **70**, 2767 (1996).
[16] E. D. Sheets, G. M. Lee, R. Simson, and K. Jacobson, Biochemistry **36**, 12449 (1997).
[17] P. R. Smith, I. E. G. Morrison, K. M. Wilson, N. Fernandez, and R. J. Cherry, Biophys. J. **76**, 3331 (1999).
[18] E. B. Brown, E. S. Wu, W. Zipfel, and W. W. Webb, Biophys. J. **77**, 2837 (1999).
[19] M. J. Saxton, Biophys. J. **66**, 394 (1994).
[20] M. J. Saxton, Biophys. J. **70**, 1250 (1996).
[21] K. Kang and S. Redner, Phys. Rev. A **32**, 435 (1985).
[22] B. I. Henry and S. L. Wearne, Physica A **276**, 448 (2000).
[23] B. I. Henry and S. L. Wearne, SIAM J. Appl. Math. **62**, 870 (2002).
[24] M. O. Vlad and J. Ross, Phys. Rev. E **66**, 061908 (2002).
[25] S. Fedotov and V. Mendez, Phys. Rev. E **66**, 030102(R) (2002).
[26] J. Sung, E. Barkai, R. J. Silbey, and S. Lee, J. Chem. Phys. **116**, 2338 (2002).
[27] B. I. Henry, T. A. M. Langlands, and S. L. Wearne, in *Proceedings of the First International Workskshop on Fractional Differentiation and it's Applications* edited by A. Le Mehauté, J. T. Machado, J. Trigeassou and J. Sabatier (International Federation of Automatic Control, Bordeaux, France, 2004), pp. 113–120.
[28] M. Fukunaga, in *Proceedings of the First International Workskshop on Fractional Differentiation and it's Applications* edited by A. Le Mehauté, J. A. Tenreiro Machado, J. C. Trigeassou, and J. Sabatier (International Federation of Automatic Control, Bordeaux, France, 2004), pp. 558–563.
[29] V. Méndez, D. Campos, and J. Fort, Phys. Rev. E **69**, 016613 (2004).
[30] D. del-Castillo-Negrete, B. A. Carreras, and V. E. Lynch, Phys. Rev. Lett. **91**, 018302 (2003).
[31] K. Seki, M. Wojciki, and M. Tachiya, J. Chem. Phys. **119**, 2165 (2003).
[32] K. Seki, M. Wojciki, and M. Tachiya, J. Chem. Phys. **119**, 7525 (2003).
[33] S. B. Yuste, L. Acedo, and K. Lindenberg, Phys. Rev. E **69**, 036126 (2004).
[34] A. Gierer and H. Meinhardt, Kybernetika **12**, 30 (1972).
[35] I. Prigogine and R. Lefever, J. Chem. Phys. **48**, 1695 (1968).
[36] C. Varea and R. A. Barrio, J. Phys.: Condens. Matter **16**, S5081 (2004).
[37] M. Weiss, Physica D **99**, 303 (1996).
[38] E. Montroll and G. Weiss, J. Math. Phys. **6**, 167 (1965).
[39] M. F. Shlesinger, J. Stat. Phys. **10**, 421 (1974).
[40] J. Klafter, A. Blumen, and M. F. Shlesinger, Phys. Rev. A **35**, 3081 (1987).
[41] A. Compte, Phys. Rev. E **53**, 4191 (1996).
[42] R. Metzler and J. Klafter, Phys. Rep. **339**, 1 (2000).

[43] R. Metzler and J. Klafter, J. Phys. A **37**, R161 (2004).
[44] E. Barkai, R. Metzler, and J. Klafter, Phys. Rev. E **61**, 132 (2000).
[45] I. Podlubny, *Fractional Differential Equations Vol. 198 of Mathematics in Science and Engineering* (Academic Press, New York, 1999).
[46] T. A. M. Langlands and B. I. Henry, J. Comput. Phys. **205**, 719 (2005).
[47] B. I. Henry, S. L. Wearne, and T. A. M. Langlands, UNSW Appl. Math. Rep. **AMR05/3** (2005).
[48] A.-L. Barabasi and H. E. Stanley, *Fractal Concepts in Surface Growth* (Cambridge University Press, Cambridge, England, 1995).
[49] P. Meakin, *Fractals, Scaling and Growth far from Equilibrium* (Cambridge University Press, Cambridge, England, 1998).
[50] B. B. Mandelbrot and J. R. Wallis, Water Resour. Res. **5**, 260 (1969).
[51] G. Moreira, J. Kamphorst, L. de Silva, and S. O. Kamphorst, J. Phys. A **27**, 8079 (1994).
[52] T. Kosztolowicz, K. Dworecki, and S. Mrowczynski, Phys. Rev. E **71**, 041105 (2005).
[53] K. B. Oldham and J. Spanier, *The Fractional Calculus: Theory and Applications of Differentiation and Integration to Arbitrary Order Vol. 111 of Mathematics in Science and Engineering* (Academic Press, New York, 1974).
[54] W. H. Press, S. A. Teukolsky, W. T. Vetterling, and B. P. Flannery, *Numerical Recipes in Fortan 77–The Art of Scientfic Computing*, 2nd ed. (Cambridge University Press, New York, 1996).